International Symposium
On Turbulence and Shear Flow
Phenomena (TSFP-9)
June 30 - July 3, 2015 *Melbourne, Australia*

SENSOR-BASED ESTIMATION OF THE VELOCITY IN THE HIGHLY MODULATED WAKE OF A WALL-MOUNTED PYRAMID

Zahra Hosseini, Robert J. Martinuzzi
Department of Mechanical and Manufacturing Engineering
Schulich School of Engineering, University of Calgary
2500 University Drive NW, Calgary, Alberta, T2N 1N4, Canada
zhossein@ucalgary.ca, rmartinu@ucalgary.ca

Bernd R. Noack
Institut PPRIME, CNRS – Université de Poitiers – ENSMA
UPR 3346, Département Fluides, Thermique, Combustion, CEAT
43 rue de l'Aérodrome, F-86036 POITIERS Cedex, France
bernd.noack@univ-poitiers.fr

ABSTRACT

A methodology for improved sensor-based velocity field estimation from experimental data in bluff-body wakes is presented and illustrated for the turbulent wake of a wall-mounted square-base pyramid. The sensors monitor the local surface pressure, while the velocity field is measured with planar, time-resolved stereoscopic PIV. Starting from the extended proper orthogonal decomposition technique, key improvements of the spatio-temporal resolution of the strongly modulated shedding include: (1) exploiting the guaranteed orthogonality of the velocity expansion modes; (2) using explicit modal cross-correlations between velocity and pressure fields; (3) determining objectively sensor-signal time delays; and (4) benefiting from symmetry considerations. Combined, these filtering operations yield a near-optimal estimation from surface pressure signals. It is shown that the mean-field paraboloid is better rendered and the residual of the estimated coherent kinetic energy is 30% - 50% smaller than with previously proposed estimation methods.

INTRODUCTION

Estimation of the velocity field from remote sensors, such as wall pressures, is a valuable tool for constructing a global estimation of the temporal and spatial evolution of the most energetic coherent structures, such as shed vortices. Typically, the signals from a few fixed sensors at flow-domain boundaries (*i.e.* remote-sensors) are used to synchronize the coherent contributions to the velocity field fluctuations obtained from uncorrelated (independent) measurements. Since the strain field distorts these structures, it is critical to capture with fidelity the temporal relationship between the remote sensor and the velocity fluctuation throughout the flow domain.

Estimation is an important tool in numerous applications. Generally, estimators are integral parts of many control strategies. Moreover, a simulation of a configuration may be used to calibrate an estimator for *in situ* monitoring based on a remote-sensor. These techniques are very useful for the purpose of global reconstructions from uncorrelated velocity measurements, such as those obtained from separate domains using particle image velocimetry (PIV). More fundamentally, it is possible to investigate from these reconstructed fields the global dynamics of coherent motions in turbulent wakes as a step towards understanding or modelling inter-scale energy transfer. It remains, however, that the rendering of global dynamics is challenging. Herein, several modifications to the extended proper orthogonal decomposition EPOD (Borée, 2003) are presented for the purpose of improving the representation of the global dynamics from sensor-based estimations.

EPOD, a variant of the linear stochastic estimation (LSE) technique of Adrian & Moin (1988), uses the sensor POD coefficients with the velocity data for estimation. If all sensor modes are used, EPOD reduces to LSE (Borée, 2003). These techniques have proven effective for studying pressure-velocity correlations. Nevertheless, for highly modulated quasi-periodic turbulent as considered here and given generally limited information from experiments, both techniques inconsistently render key elements of the flow dynamics: the temporal evolution of energetic content and the synchronization between different scales of motion.

An improvement to the synchronization between the sensor signal and the velocity field for estimation purposes can be obtained using the multi-time-delay technique (Durgesh & Naughton, 2010) in combination with LSE or EPOD. When carefully used, this approach results in better estimation of the periodic component of the velocity field. However, its implementation presents some challenges. The quality of the estimation generally depends on using an empirically determined optimal number of sensor signal modes. More significantly, the estimated velocity modes are non-orthogonal such that only the dominant (most energetic) velocity mode is synchronized with the sensor signal.

The method proposed here is an improvement of the EPOD technique aimed at optimizing the estimation by maximizing the surface pressure-velocity correlation. To this end, the velocity field is expanded onto an optimal orthogonal basis, thereby reducing the spatio-temporal corre-

lations of the EPOD approach to purely temporal correlations. With this great simplification, it is possible to easily detect and extract the existing correlations and develop different treatments to improve the estimator (pressure) and estimated (velocity) fields by recovering the phase relationships between pressure and velocity POD modes. Taking advantage of symmetries, the optimal space is defined following a procedure similar to Bourgeois *et al.* (2013).

An experimental study of the wake flow for a surface-mounted, square-based pyramid is used as a heuristic case. Highly three-dimensional quasi-periodic wakes are generally observed for surface-mounted tapered bluff bodies protruding a boundary layer. For low-aspect ratio (apex angles between 15° and 70°) tapered flat plates (Castro & Watson, 2004) and pyramids (Martinuzzi, 2008), coherent structures are shed at a frequency scaled with the base width. Similarly to cone geometries (Gaster, 1969), the shed structures are highly distorted resulting in a low-frequency drift and phase jitter. It will be shown that the proposed method captures the these modulations with the correct synchronization to account for the spatial distortion of the shed vortices and thus reliably render the dynamic behaviour.

EXPERIMENTAL SET-UP

The measurements were done in a suction type open-test-section wind tunnel. The geometry and nomenclature are schematically shown in Fig. 1. A square-base pyramid of height $h = 39mm$ and width $d = 45mm$ (apex angle $\xi = 60°$) was mounted on a flat plate with a sharp leading edge. The thickness of the boundary layer with the pyramid removed was $\delta/h = 0.25$ as shown in Fig. 2. The free-stream velocity was $U_\infty = 10m/s$, corresponding to a Reynolds number $Re_d = U_\infty d/\nu = 28{,}000$, where ν is the kinematic viscosity of air. The free-stream turbulence intensity was approximately 0.8%.

A LaVision Flow Master planar stereoscopic PIV system was used to measure the velocity vectors (u,v,w) along horizontal $(x-y)$ planes. The light source was a Photonics Industries 15mJ 527nm Nd-YLF pulsed laser. Image pairs were acquired with 2 Photron Fastcam SA4 cameras with an image-pair time separation of 18μs at a rate of 500Hz, capturing approximately 10 data points per shedding cycle. Interrogation windows of 32×32 pixels with 50% overlap (giving a vector spacing of 1.2mm) were used to calculate the velocity vectors. For each plane, at least 6,000 image pairs were obtained spanning 600 shedding cycles.

The fluctuating pressure at the pyramid side faces ($z/h = 0.22, 0.45, 0.68$ at both faces) and the flat plate ($x/d = 1.5, 2$ and $y/d = \pm 0.25$) were taken simultaneously with the velocity data at a sampling rate of 10.24kHz.

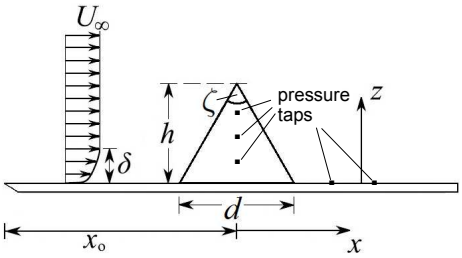

Figure 1. Schematic of geometry and nomenclature.

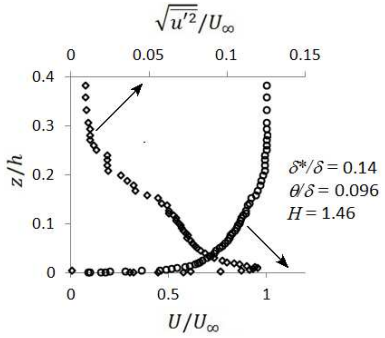

Figure 2. Boundary layer profile and root-mean-square velocity. The displacement thickness δ^*, momentum thickness θ and shape factor $H = \delta^*/\theta$ are also shown.

Flow Characteristics

Representative velocity and surface pressure time series and their corresponding power spectral density (PSD) functions are shown in Fig. 3. Similar behaviour is observed in both fields. The spectral peak associated with quasi-periodic vortex shedding occurs at a non-dimensional (Strouhal) frequency of $St_d = f_c d/U_\infty = 0.231 \pm 0.005$. Note the high modulation of the amplitude and the signal short-term average (black line). The short term average is obtained using a Gaussian filter defined in (1):

$$\langle u \rangle_G(t) = \int_{-\infty}^{\infty} u(\tau)\, g(t-\tau)\, d\tau, \;\; g(t) = \frac{1}{\sqrt{2\pi}\sigma} e^{-\frac{t^2}{2\sigma^2}}. \quad (1)$$

The bandwidth of the filter, σ is based on the integral time-scale, $1/f_\tau$, corresponding to the first zero of the autocorrelation function of the most energetic symmetric non-harmonic POD mode from the unfiltered data. This mode corresponds to a short-term average slow drift (Holmes *et al.*, 2012). Here $f_\tau \approx f_c/6$ and, by the Nyquist theorem, the filter cut-off frequency is set to $2f_\tau$ yielding a bandwidth $\sigma = \sqrt{1/6}/f_c$.

FLOW ESTIMATION

As a starting point, the salient features of EPOD (Borée, 2003) are reiterated for continuity. First, the spatio-temporal pressure data acquired at locations $\mathbf{X}$ from N_p sensors are expanded onto the orthonormal basis: $p(\mathbf{X},t) = \sum_{n=1}^{N_p} a_p^{(n)}(t)\phi_p^{(n)}(\mathbf{X})$, where $a_p^{(n)}(t)$ and $\phi_p^{(n)}(X)$ denote the nth temporal coefficient and spatial eigenvectors, respectively. The extended velocity modes are then defined: $\psi_u^{(n)}(\mathbf{x}) = \langle a_p^{(n)}(t)\mathbf{u}(\mathbf{x},t)\rangle/\lambda_p^{(n)}$, where $\langle\cdot\rangle$ denotes teh time-averagig operator; $\lambda_p^{(n)} = \langle a_p^{(n)}(t)a_p^{(n)}(t)\rangle$ and $\mathbf{x}$ are locations in the velocity field. Note the $\psi_u^{(n)}(\mathbf{x})$ are generally not orthogonal. The velocity, then, is estimated using:

$$\hat{\mathbf{u}}(\mathbf{x},t_{est}) = \sum_{n=1}^{N_{mode}} a_p^{(n)}(t_{est})\, \psi_u^{(n)}(\mathbf{x}) \quad (2)$$

where t_{est} denotes the time in the trial data set and $N_{mode} = N_p$ if all extended modes are used.

Here, the EPOD technique is modified to optimize the estimation by extracting the maximum pressure-velocity correlations, with pressure sensors presumably not located

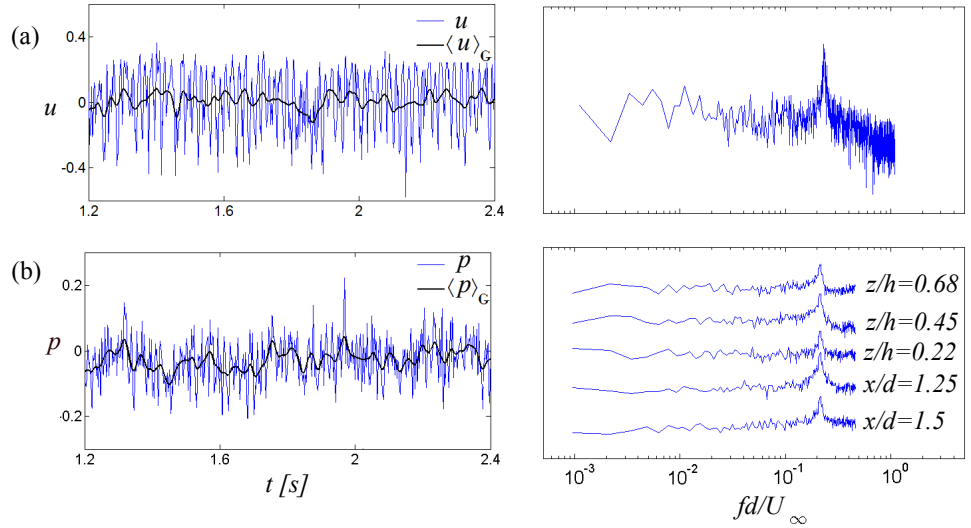

Figure 3. Representative fluctuating velocity at (a) $x/d = 2.25, y/d = 0.30, z/h = 0.70$, and (b) pressure taken simultaneously. The Power Spectral Density functions are shown on the right and are offset for clarity.

in the optimum positions as these have been chosen with limited *a priori* information about the flow. To this end, modifications are made in four respects: (1) change the estimation basis to an optimal orthonormal basis; (2) use sensor history to recover velocity cyclical behaviour; (3) fix the phase of the slow-drift mode and (4) improve estimations of the higher harmonics. The methodology is described in detail in (Hosseini *et al.*, 2015) and is briefly summarized here.

1. Expansion onto the optimal basis: The fluctuating velocity component is expanded with a basis which, by construction, is orthonormal following the procedure depicted in Fig. 4. Briefly, after subtraction of the time-averaged mean, the fluctuations are decomposed in symmetric and anti-symmetric fields according to (w is treated as u):

$$
\begin{aligned}
u_s(x,y,z,t) &= [u(x,y,z) + u(x,-y,z)]/2, \\
u_a(x,y,z,t) &= [u(x,y,z) - u(x,-y,z)]/2, \\
v_s(x,y,z,t) &= [v(x,y,z) - v(x,-y,z)]/2, \\
u_a(x,y,z,t) &= [v(x,y,z) + v(x,-y,z)]/2.
\end{aligned}
$$

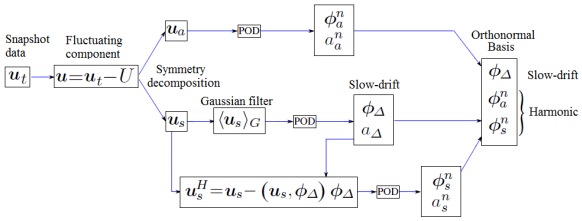

Figure 4. Algorithm used to obtain the orthonormal subspace onto which the velocity data is expanded.

This decomposition confers beneficial convergence behaviour fo the spatial modes (Holmes *et al.*, 2012), which is paramount to the accuracy of the estimation. The benefits have been verified to outweigh the potential risk due to crosstalk arising from experimental uncertainty.

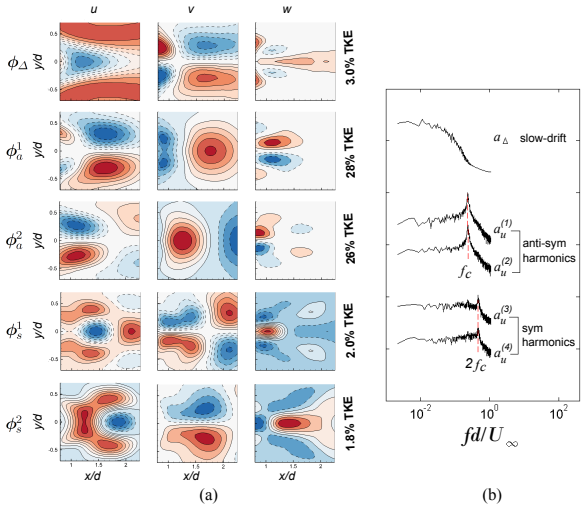

Figure 5. (a) Contours the velocity spatial modes at the plane $z/h = 0.23$. The dashed lines indicate negative values. Subscripts a, s and Δ indicate the anti-symmetric, symmetric and slow-drift modes, respectively. (b) The Power Spectral Density functions of the corresponding temporal coefficients. Spectra are offset for clarity.

The anti-symmetric harmonic modes are determined from a POD of the anti-symmetric field. The symmetric field is decomposed into slow and fast-varying parts. The slow-varying part is calculated using the Gaussian operator of (1). The most energetic mode is taken to represent the low frequency base-flow variations (slow-drift mode). The fast-varying component is the leftover from the symmetric field. POD is performed on this field to obtain symmetric harmonic modes.

The five most energetic modes in the plane $z/h = 0.23$ are shown in Fig. 5. The two most energetic modes correspond to the anti-symmetric harmonic pair with frequency f_c, while the symmetric field yields the second harmonic ($2f_c$). Note that this mathematical method does not require this similarity to temporal Fourier modes. The third most energetic mode is the slow-drift mode.

By expanding the velocity data onto the orthonormal

basis as in (3), the correlations between the spatio-temporal velocity data and the pressure coefficients, $\psi_u^{(n)}$ reduce to correlations between the temporal coefficients as per (4):

$$\hat{\mathbf{u}}(\mathbf{x},t_{est}) = \sum_{k=1}^{N_u} \hat{a}_u^{(k)}(t_{est})\,\phi_u^{(k)}(\mathbf{x}) \tag{3}$$

$$\hat{a}_u^{(k)}(t_{est}) = \sum_{n=1}^{N_{mode}} a_p^{(n)}(t_{est})\,\frac{\left\langle a_p^{(n)}(t)\,a_u^{(k)}(t)\right\rangle}{\lambda_p^{(n)}} \tag{4}$$

where $\phi_u^{(k)}(\mathbf{x})$ and $a_u^{(k)}(t)$ are, respectively, eigenmodes and their corresponding temporal coefficients. This great simplification significantly reduces the computational effort and makes it possible to explicitly detect and extract the existing correlations in given data. Only the pressure modes for which the correlation with the velocity field is non-vanishing are used in the estimation. Hence, this approach eliminates the need for additional ranking criteria for selection and reduces the experimental uncertainty introduced by including non-contributing modes: *cf.* Sicot *et al.* (2012); Clark *et al.* (2014). Here, when considering only the non-vanishing correlations, the estimation of the velocity coefficients for the first harmonic pair ($k = 1,2$) and the slow-drift Δ reduce to

$$\begin{aligned}\hat{a}_u^{(k)}(t_{est}) &= a_p^{(1)}(t_{est})\,\frac{\left\langle a_p^{(1)}(t)\,a_u^{(k)}(t)\right\rangle}{\lambda_p^{(1)}} \\ &\quad + a_p^{(2)}(t_{est})\,\frac{\left\langle a_p^{(2)}(t)\,a_u^{(k)}(t)\right\rangle}{\lambda_p^{(2)}}, \\ \hat{a}_\Delta(t_{est}) &= a_p^{G}(t_{est})\,\frac{\left\langle a_p^{G}(t)\,a_\Delta(t)\right\rangle}{\lambda_p^{G}}.\end{aligned} \tag{5}$$

2. Sensor history for harmonic mode estimation: The correlations between the pressure and velocity coefficients are improved by forcing the convergence of the pressure modes using the multi-time-delay approach (Lasagna *et al.*, 2013). This approach also conveniently accounts for the phase shift between the pressure and velocity harmonic coefficients (Durgesh & Naughton, 2010). Briefly, the spatial information of the sensor data is obtained by treating the time-delayed signal as originating from virtual sensors located downstream of the physical sensor at location $\mathbf{X}_1$. The pressure of the mth virtual sensor $p_{m+1}(\mathbf{X}_m,t)$ is statistically similar to that of the phsyical sensor, but delayed by $m\Delta\tau$: $p_{m+1}(\mathbf{X}_m = \mathbf{X}_1 - m\Delta\mathbf{X},t) = p_1(\mathbf{X}_1,t-m\Delta\tau)$, where $\Delta\mathbf{X} = \mathbf{U}_c\Delta\tau$. $\mathbf{U}_c$ is a characteristic convection velocity, but its exact definition is not needed as it is absorbed when normalizing the POD modes. For N physical sensors, and M time-delayed signals, the POD is performed for a system of $N_p = N\times(M+1)$ sensors.

In earlier LSE and EPOD studies of turbulent flows, it has been shown that therre is an optmal value for the maximum time delay $\tau_T = M\Delta\tau$ above which the estimation deteriorates: Durgesh & Naughton (2010); Sicot *et al.* (2012). These parameters are usually selected empirically based on various performance measures (Clark *et al.*, 2014).

Criteria are proposed herein for selecting τ_T, M and consequently $\Delta\tau$. Intuitively, the addition of more time-delayed signals results in mostly redundant data since periodic information is simply repeated. Hence, the optimal time delay should be $\tau_T \approx 1/f_c$. Hosseini *et al.* (2015) show that 4 points per cycle are sufficient to resolve a harmonic mode. Thus to resolve both the first and second harmonics (average frequency f_c and $2f_c$, respectively), five points per second-harmonic cycle over the first-harmonic period was implemented: *viz:* $\Delta\tau = 1/_{10f_c}$ and $M = 10$.

The error between the estimated coefficients of the first harmonic pair and the actual coefficients is shown in Fig. 6 for a time-delay of $\tau_T = 1/f_c$ and various M. Three independent experimental trials (measurements) were conducted. The first two were used to determine the correlation coefficients and POD velocity modes. The third trial was then estimated. The error is defined as in Durgesh & Naughton (2010): the sum of errors for each coefficient normalized by the respective energy $\varepsilon = \left\langle \sqrt{(\hat{a}_u^{(1)} - a_u^{(1)})^2/2\lambda_1 + (\hat{a}_u^{(2)} - a_u^{(2)})^2/2\lambda_2} \right\rangle$. A significant improvement is achieved when the optimal M is used compared to the single-time estimation. Moreover, the error is not reduced by using a smaller time-interval (larger M).

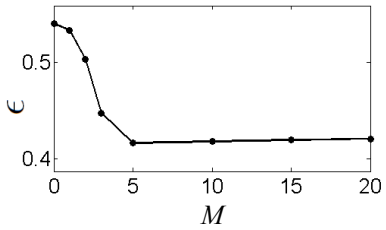

Figure 6. The error, ε, of estimated coefficients for the first harmonic pair for $\tau_T = 1/f_c$ as a function of number of time-delayed signals, M.

3. Fixing the phase of the slow-drift mode: The estimation of the velocity field is improved by including a time delay for the non-harmonic modes separately. Omitting this step introduces an artificial and random phase lag between the non-harmonic and harmonic fluctuations; resulting in a misrepresentation of the coherent strain field and the dynamics of the coherent motion. For the slow-drift mode, the time delay τ_Δ is found from the peak of the cross-correlation function of the pressure, a_p^G, and the velocity, a_Δ, coefficients. The correct phase in the estimation $\hat{a}_\Delta$ is recovered as shown in (6).

$$\hat{a}_\Delta(t_{est}) = a_p^G(t_{est}-\tau_\Delta)\,\frac{\left\langle a_p^G(t-\tau_\Delta)\,a_\Delta(t)\right\rangle}{\lambda_p^G}. \tag{6}$$

4. Estimation of higher harmonics: A Galerkin projection of the Navier-Stokes equations on to the five most energetic modes indicates that the second-harmonic coefficients are related to the first-harmonic coefficients through Reynolds stress-like terms (Bourgeois *et al.*, 2013; Holmes *et al.*, 2012).The slow-drife mode is found empirically to be uncorrelated to the second-harmonic coefficients. Thus, taking advantage of the proposed orthogonal representation of (3), the second harmonic coefficients can be estimated according to (7):

$$\begin{aligned}\hat{a}_u^{(k)} = \ell_{k11}a_p^{(1)}a_p^{(1)} &+ \ell_{k22}a_p^{(2)}a_p^{(2)} + \ell_{k12}a_p^{(1)}a_p^{(2)} \\ &+ q_{k3}a_p^{(3)} + q_{k4}a_p^{(4)}\end{aligned} \tag{7}$$

where $k = 3,4$ denote the second harmonic modes of velocity and ℓ_{kij} , q_{ki} are the correlation coefficients. The phase for the second harmonic is accounted for through the implemented variation of the multi-time-delay approach.

Results

Comparisons are conducted to evidence th estimation improvements achieved through the proposed modifications. In the following, EPOD refers to the traditional technique using all available pressure modes. The next three methods use only the five most energetic modes: EPOD-OB using the orthonormal basis of (3); EPOD-MTD using the multi-time-delay technique with optimal number of virtual sensors and NEW for the proposed methodology, which also includes phase-delays for non-harmonic modes and (7).

The measured and estimated velocity coefficients in the $(a_u^{(1)}, a_u^{(2)}, a_\Delta)$space are shown in Fig. 7 for a representative cycle in the plane $z/h = 0.23$. The limit cycle behaviour is not recovered in the $(a_u^{(1)}, a_u^{(2)}, a_\Delta)$ space using traditional EPOD or EPOD-OB. The latter shows a better estimation of the slow-drift coefficient a_Δ because of the cleaner modes extracted through the use of symmetry and the orthonormal projection. A significant improvement is achieved using the multi-time-delay (EPOD-MDT) approach in recovering the limit-cycle behaviour, but the estimated magnitude $\hat{a}_\Delta$ is significantly separated from the measured one.

Omitting the time shift τ_Δ between the harmonic and slow-drift modes results in a poor estimation of a_Δ as is clearly evident when comparing the estimated $\hat{a}_\Delta$ and measured a_Δ as a function of the estimator a_p^G as in Fig. 8a. However, using $\tau_\Delta = 0.7/f_c$ as determined from the pressure-velocity slow-drift cross-correlations as shown in Fig. 8c, the estimate $\hat{a}_\Delta$ using the NEW proposed approach much more closely follows a_Δ as seen in Fig. 8b. It is immediately seen from Fig. 7b, that the estimation for the first-harmonic velocity coefficients follow more closely the measured trajectory in the phase-space as a result of correctly recovering the phase of the slow-drift coefficient.

The optimality of the estimation is better indicated by comparing the flow estimation $\hat{\mathbf{u}}$ with the best achievable resolution $\mathbf{u}_c$ by projecting the measured flow on the same five-mode subspace:

$$R_c = \frac{\int_{\mathbf{x}} (\mathbf{u}_c - \hat{\mathbf{u}}) \,.\, (\mathbf{u}_c - \hat{\mathbf{u}})\, d\mathbf{A}}{\left\langle \int_{\mathbf{x}} \mathbf{u}_c \,.\, \mathbf{u}_c \, d\mathbf{A} \right\rangle}.$$

As seen in Fig. 9, the error in the estimation is significantly reduced from $\sim 30\%$ using EPOD, to about 18% with EPOD-MTD and $\sim 16\%$ with the NEW procedure.

The proposed methodology improves the rendering of the flow topology and coherent motion as is illustrated in Fig. 10. Here, the estimated sectional streamlines and vortex core regions are compared to those for the measured field for a randomly selected PIV snapshot in the plane $z/h = 0.23$. Although the energetic content of a_Δ is relatively small, its synchronization is critical and has important consequences, for example, the better capture of the location of the saddle point **S**, the curvature of contingent streamlines and the location of the focus **F**. Moreover, a better estimation of the second harmonics using the proposed NEW method improves the estimation of the shed vortex $\mathbf{V_s}$ especially in regions close to the centreline.

The scatter plot in the $(a_u^{(1)}, a_u^{(2)}, a_\Delta)$ space for EPOD-MDT and the NEW methods are compared to measured data in Fig. 11 for the plane $z/h = 0.23$. The trajectories are shown for two randomly selected sample time-intervals each spanning approximately one shedding cycle. While both methods yield a mean field paraboloid, the trajectory using EPOD-MDT is inconsistently over or underestimated. The estimation from NEW method, on the other hand, closely follows the correct path along the vertical axis (a_Δ axis). Correctly estimating the trajectory in the mean field paraboloid is of critical importance in capturing the flow dynamics. From a technique perspective, the temporal relationship between the slow-drift and harmonic components is a key element in synchronizing uncorrelated PIV measurements to obtain a physically representative reconstruction of the flow field (Bourgeois *et al.*, 2013). Fundamentally, and perhaps more significantly, this relationship between slow-drift and harmonic coefficients expresses the energy transfer between these modes and must be correctly captured for meaningful analysis (Holmes *et al.*, 2012).

Concluding Remarks

A systematic and objective methodology to extract the pressure-velocity correlations for the velocity estimation in highly modulated quasi-periodic wakes is proposed. We show how physically motivated spatial and temporal filters of the pressure and velocity fields improve the estimation as measured in terms of resolved fluctuation energy and achieved residuals. Most significantly, the dynamic behaviour is well captured in the modal subspace. This 2D

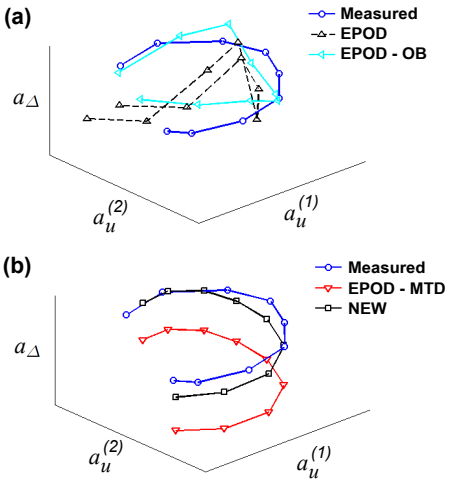

Figure 7. Behaviour of a typical cycle in $(a_u^{(1)}, a_u^{(2)}, a_\Delta)$ space in the plane $z/h = 0.23$.

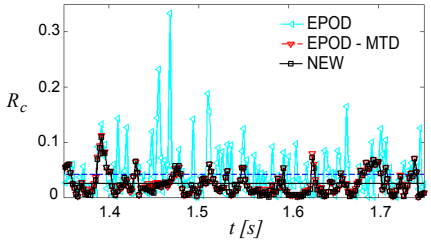

Figure 9. Residual of coherent contributions to velocity field in plane $z/h = 0.23$. Horizontal line shows average.

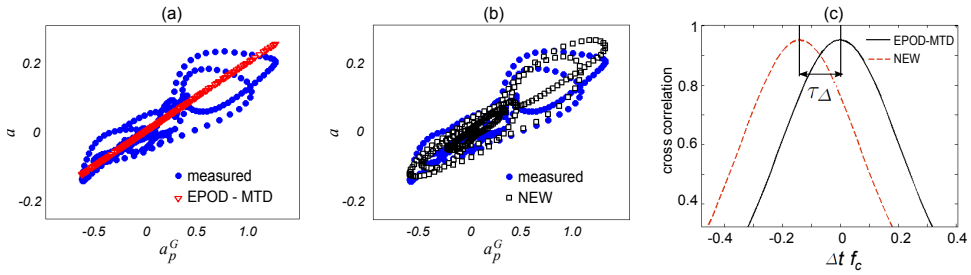

Figure 8. Comparison of measured and estimated velocity slow-drift coefficient a_Δ *vs.* pressure coefficient a_p^G for a) EPOD-MTD and b) NEW procedures, respectively. c) $a_\Delta - a_p^G$ Cross-correlation function.

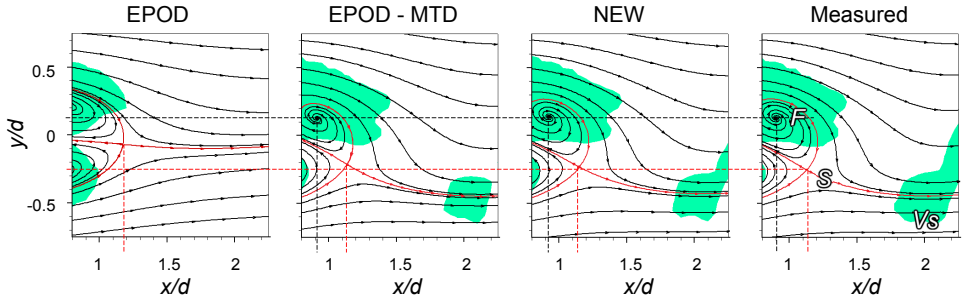

Figure 10. Estimated and measured sectional streamlines and vortex core (using λ_2-criterion) in the plane $z/h = 0.23$

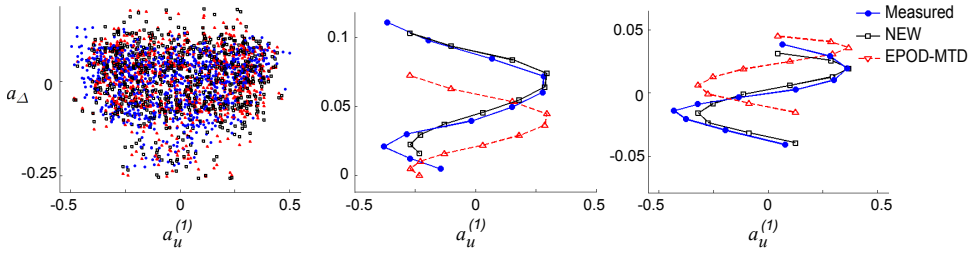

Figure 11. Scatter plot and trajectory of two sample cycles from measured and estimated velocity file for plane $z/h = 0.23$.

estimation tool can be used to construct 3D time-variant velocity fields, similar to Bourgeois *et al.* (2013), and thus is useful for exploring fundamental aspects of dynamics. Key enablers for the improved methodology are: a careful reconstruction of an orthonormal velocity basis; noise truncation by a suitable subspace; introducing optimal time delay between sensor and flow for both harmonic and non-harmonic contributions and better estimation of the higher-harmonics.

REFERENCES

Adrian, R. J. & Moin, P. 1988 Stochastic estimation of organized turbulent structure : homogeneous shear flow. *Journal of Fluid Mechanics* **190**, 531–559.

Borée, J. 2003 Extended proper orthogonal decomposition: a tool to analyse correlated events in turbulent flows. *Experiments in Fluids* **35**, 188–192.

Bourgeois, J. A., Noack, B. R. & Martinuzzi, R. J. 2013 Generalized phase average with applications to sensor-based flow estimation of the wall-mounted square cylinder wake. *Journal of Fluid Mechanics* **736**, 316–350.

Castro, I. P. & Watson, L. 2004 Vortex shedding from tapered, triangular plates: taper and aspect ratio effects. *Experiments in Fluids* **37**, 159–167.

Clark, H., Naghib-Lahouti, A. & Lavoie, P. 2014 General perspectives on model construction and evaluation for stochastic estimation, with application to a blunt trailing edge wake. *Experiments in Fluids* **55**, 1756.

Durgesh, V. & Naughton, J. W. 2010 Multi-time-delay LSE-POD complementary approach applied to unsteady high-Reynolds-number near wake flow. *Experiments in Fluids* **49**, 571–583.

Gaster, M. 1969 Vortex shedding from slender cones at low Reynolds numbers. *Journal of Fluid Mechanics* **38**, 565–576.

Holmes, P., Lumley, J. L., Berkooz, G. & Rowley, C. W. 2012 *Turbulence, coherent structures, dynamical systems and symmetry*, 2nd edn. University Press, Cambridge: Cambridge Monographs on Mechanics.

Hosseini, Z., Martinuzzi, R. J. & Noack, B. R. 2015 Sensor-based estimation of the velocity in the wake of a low-aspect-ratio pyramid. *Experiments in Fluids* **56**, 13.

Lasagna, Davide, Orazi, Matteo & Iuso, Gaetano 2013 Multi-time delay, multi-point linear stochastic estimation of a cavity shear layer velocity from wall-pressure measurements. *Physics of Fluids* **25** (1), 017101.

Martinuzzi, R. J. 2008 Dual vortex structure shedding from low aspect ratio, surface-mounted pyramids. *Journal of Turbulence* **28**, 1–16.

Sicot, C., Perrin, R., Tran, T. T. & Borée, J. 2012 Wall pressure and conditional flow structures downstream of a reattaching flow region. *International Journal of Heat and Fluid Flow* **35**, 119–129.